

A Single-Emitter Gain Medium for Bright Coherent Radiation from a Plasmonic Nanoresonator

Pu Zhang¹, Igor Protsenko², Vahid Sandoghdar³, and Xue-Wen Chen^{1*}

¹School of Physics, Huazhong University of Science and Technology, Luoyu Road 1037, Wuhan, 430074, People's Republic of China

²Lebedev Physical Institute, Leninsky prospect 53, Moscow, 119991, Russia

³Max Planck Institute for the Science of Light, Staudtstr. 2, D-91058 Erlangen, Germany

Abstract

We theoretically demonstrate the generation and radiation of coherent nanoplasmons powered by a single three-level quantum emitter on a plasmonic nanoresonator. By pumping the three-level emitter in a Raman configuration, we show a pathway to achieve macroscopic accumulation of nanoplasmons due to stimulated emission in the nanoresonator despite their fast relaxation. Thanks to the antenna effect of the nanoresonator, the system acts as an efficient and bright nanoscopic coherent light source with a photon emission rate of hundreds of Terahertz and could be realized with solid-state emitters at room temperatures in pulse mode. We provide physical interpretations of the results and discuss their realization and implications for ultra-compact integration of optoelectronics.

PACS numbers: 42.50.Ar, 42.50.Pq, 42.55.-f, 73.20.Mf

* Correspondence should be addressed to X.-W. C. (email: xuewen_chen@hust.edu.cn).

Conventional lasers have dimensions larger than or comparable to the wavelength of the emitted light and contain a large number of active emitters [1]. In recent years there has been great interest in developing subwavelength lasers both from a fundamental point of view and the perspective of device miniaturization and integration for applications [2-4]. To get around the need for an optical cavity, various nanolasers or spasers have been theoretically proposed [5-9] and experimentally demonstrated [10-16] based on plasmonic effects in one, two or three dimensions. Nevertheless, these devices require high concentrations of emitters to reach sufficient gain and overcome the dissipation loss of plasmons in metals, causing excess heat [3] or quenching due to energy transfers among the emitters at high concentration [8]. In this work, we explore and devise a type of nanoscopic coherent light source with minimal amount of gain material, namely, generation and radiation of nanoplasmons powered by only one quantum emitter on an optical antenna. The nanoscopic light source has fields concentrated at deep subwavelength scale in all three dimensions and radiates efficiently with bright photon streams at a rate of hundreds of Terahertz. We show a pathway to achieve that and elucidate the unique physics associated.

Optical antennas or plasmonic nanoresonators are metal nanostructures with localized surface plasmon resonances and can greatly enhance absorption and radiation of optical energy for a nearby quantum emitter [17]. They have been widely applied to modify spontaneous emission rate and emission pattern of single emitters [18-22]. An alternative view on optical antennas is to consider them as storage cavities with nanoscale mode volumes and low quality factors (Q) owing to high radiation and absorption loss [23-24]. In spite of their low Q s, optical antennas could provide strong enhancement of the local density of photonic states (LDOS) and, thus, lead to the so-called strong coupling between a single emitter and the nanocavity mode [25-29]. Indeed, recent experiments reported the strong coupling with vacuum Rabi splitting (VRS) in the order of 100 millielectronvolts (meV) for a single emitter [20,31]. In these systems, the emitter has a great influence on the system dynamics and may experience stimulated emission under effective pumping as in a single-atom microlaser [32-38].

In contrast to microlasers, the single-emitter nanoscopic source we introduce here is deep subwavelength scale in all three dimensions and the system dynamics is 6-8 orders of magnitude faster. Nanoplasmons on optical antennas typically have relaxation times of well below 20 fs. Such fast decay not only poses a challenge for achieving strong coupling but also presents difficulties in effective pumping of the active emitter. Indeed, the (non-)radiative relaxation rate of the excited emitter to the upper laser

level is usually a few orders of magnitude slower than the nanoplasmon decay rate. Therefore, the average number of nanoplasmons on the antenna is far less than one even when the emitter and nanoplasmons are in the strong-coupling regime. To get around this hurdle, we propose a two-pump scheme in a Raman configuration for a three-level system [39]. FIG.1 shows the energy level scheme of the emitter. The transition $|2\rangle \rightleftharpoons |1\rangle$ resonantly couples to the nanoplasmons on an optical antenna (see inset). Emitters with a similar level scheme have been studied in different contexts [36,40] and may be realized using molecules with vibronic levels [41]. In contrast to conventional lasers with one pumping channel, for instance Ω_{13} , we introduce a second pump field Ω_{23} so that the population in $|3\rangle$ can be rapidly transferred to $|2\rangle$, thus ensuring its occupation in the presence of fast coupling to the nanoplasmons. The depletion of the occupancy at $|3\rangle$ by Ω_{23} resembles in some sense stimulated-emission depletion (STED) [42], but here it is depleted to the lasing level $|2\rangle$ instead of the ground state. In this way, as the coupling between transitions $|2\rangle \rightleftharpoons |1\rangle$ and the nanoplasmons becomes strong, the occupation at $|2\rangle$ leads to macroscopic accumulation of nanoplasmons on the antenna and thereby considerable stimulated emission. The nonlinear feedback to the emitter provided by the nanoplasmons and the ample gain from the emitter via the Raman pumps bring the lasing-like features to our system, as discussed below.

For a quantitative discussion, we consider in FIG. 1 an emitter coupled to a generic bowtie antenna structure consisting of two nanocones, which provides simultaneous subwavelength field confinement and efficient radiation [43]. For the parameters used in FIG. 1, the antenna has a nanoplasmon resonance around 1.24 eV (1.0 μm vacuum wavelength) with a linewidth of $\kappa = 40$ meV, slightly depending on the gap size. We consider a Lorentzian spectral line shape for the nanoplasmon resonance, like the response

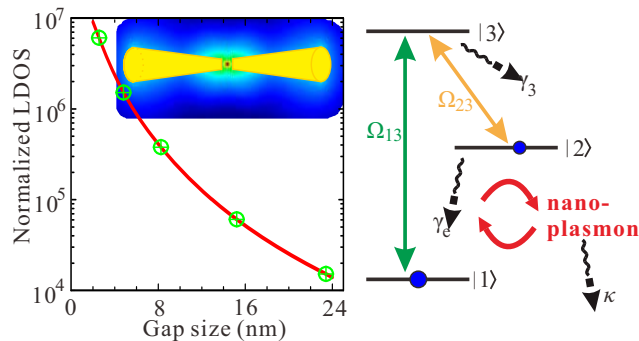


FIG. 1 (color online) The schematic of the nanoscopic coherent light source composed of a single three-level quantum emitter and an Au double-nanocone antenna. The nanocones have 20 nm base diameter, 80 nm cone length and 6 nm flat tip diameter. The trace in the left panel shows the normalized LDOS versus the gap size. The five markers from right to left correspond to coupling constant $g = 10, 20, 50, 100$ and 200 meV. The emission and pumping schemes are displayed on the right panel.

of a cavity. The trace on the left panel of FIG.1 plots ρ_L the LDOS at the gap center (where the emitter sits) normalized by the vacuum value as a function of the gap size. The radiation efficiencies of the nanoplasmons at various gap sizes are about 60%. The coupling between the nanoplasmons and the emitter is characterized by a coupling constant g , which is related to ρ_L via $g^2 = \kappa\gamma_e(\rho_L - 1)/4$ [26].

The free-space spontaneous emission rate γ_e of $|2\rangle$ is taken to be 10^9 s $^{-1}$, corresponding to 1 ns lifetime. The emitter-antenna coupled system under pumps can be treated quantum-mechanically by quantizing the nanoplasmons in the same way as photons in a cavity [27,44]. We consider a Hilbert space expanded by the emitter subspace and the Fock states of the nanoplasmons. The joint density operator $\hat{\rho}$ is a tensor product of the density matrices of the two sub-systems and evolves in time according to the master equation in Lindblad form [32, 44]:

$$\dot{\hat{\rho}} = \frac{i}{\hbar} [\hat{\rho}, \mathcal{H}_I] + \mathcal{L}\{\sqrt{\gamma_e}\hat{\sigma}_{12}\} + \mathcal{L}\{\sqrt{\gamma_3}\hat{\sigma}_{23}\} + \mathcal{L}\{\sqrt{\gamma_{de}}\hat{\sigma}_{22}\} + \mathcal{L}\{\sqrt{\kappa}\hat{a}\} , \quad (1)$$

where the system Hamiltonian with rotating wave approximation in the interaction picture reads

$$\mathcal{H}_I = \hbar g(\hat{a}^\dagger \hat{\sigma}_{12} + \hat{\sigma}_{21} \hat{a}) + \frac{1}{2}\hbar\Omega_{13}(\hat{\sigma}_{13} + \hat{\sigma}_{31}) + \frac{1}{2}\hbar\Omega_{23}(\hat{\sigma}_{23} + \hat{\sigma}_{32}) \quad (2)$$

and the Lindblad superoperator which accounts for the various dissipations is defined as

$$\mathcal{L}\{\hat{\mathbf{O}}\} = \hat{\mathbf{O}}\hat{\rho}\hat{\mathbf{O}}^\dagger - \frac{1}{2}(\hat{\mathbf{O}}^\dagger\hat{\mathbf{O}}\hat{\rho} + \hat{\rho}\hat{\mathbf{O}}^\dagger\hat{\mathbf{O}}) . \quad (3)$$

Here $\hat{\sigma}_{ij}$ is the atomic operator $|i\rangle\langle j|$. \hat{a} and \hat{a}^\dagger are the annihilation and creation Bose-operators for the nanoplasmons. We consider here for simplicity that the emitter is resonantly pumped by two coherent fields with respective Rabi frequencies of Ω_{13} and Ω_{23} , although in principle effective pumping can be achieved with pumps that have large detunings [39]. Similar results can also be obtained if the coherent pump Ω_{23} is replaced by an incoherent one (see Appendix). We assume that state $|3\rangle$ has a fast relaxation rate of $\gamma_3 = 10^{12}$ s $^{-1}$ to $|2\rangle$ and neglect its spontaneous decay to $|1\rangle$. Additional dephasing of state $|2\rangle$ may be present with a rate γ_{de} . The master equation can be solved numerically by truncating the Fock state subspace of the nanoplasmon. At steady state, by tracing out the atomic part of the density matrix, we can calculate the occupation of the nanoplasmon at various Fock states and find the mean nanoplasmon number as $n_{NP} = \text{Tr}(\hat{a}^\dagger \hat{a} \hat{\rho})$. The second-order intensity correlation function can be evaluated according to $g^{(2)}(\tau) = \frac{\langle \hat{a}^\dagger(0) \hat{a}^\dagger(\tau) \hat{a}(\tau) \hat{a}(0) \rangle}{\langle \hat{a}^\dagger(0) \hat{a}(0) \rangle^2}$, while the power spectrum of the nanoplasmon is

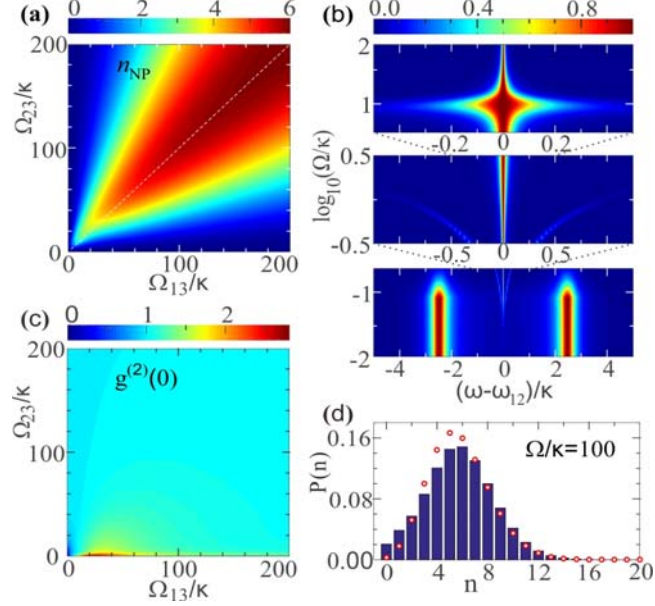


FIG. 2 (color online) Single-emitter nanoplasmon generation with $g = 100$ meV. (a) The average nanoplasmon number v.s. pump rates (dashed line: $\Omega_{23} = \Omega_{13} = \Omega$); (b) The normalized spectra of the nanoplasmon emission as a function of the pump rates Ω in logarithmic scale; (c) Second-order intensity correlation function at zero delay $g^{(2)}(0)$; (d) Fock state occupation histogram of the nanoplasmons ($\Omega = 100\kappa$) compared with Poissonian distribution (circles).

known as the Fourier transform of the first-order correlation $S(\omega) = \int_{-\infty}^{\infty} \langle \hat{a}^\dagger(\tau) \hat{a}(0) \rangle e^{-i\omega\tau} d\tau$, computed through time evolution of the master equation by the quantum regression theorem [45].

Inspired by recent experiments [30,31], we first investigate the emission properties of the emitter-antenna system in the strong-coupling regime with a coupling constant of 100 meV, corresponding to a 5 nm gap in our double-cone antenna. The color map in FIG. 2(a) displays n_{NP} as a function of the pump rates expressed in terms of κ . One clearly observes that with only one pump turned on n_{NP} is essentially zero (≤ 0.008) due to the fast decay of nanoplasmons. The generation of nanoplasmons is most effective for two pumps roughly with equal rates. This could be understood qualitatively as follows: for a given Ω_{13} , initially the increase of Ω_{23} leads to more population at $|2\rangle$ (favorable for nanoplasmon generation), and then with further increase of Ω_{23} the population is pumped out of state $|2\rangle$ (unfavorable for nanoplasmon generation) to $|1\rangle$ via $|3\rangle$. Along the white dashed line of $\Omega_{23} = \Omega_{13} = \Omega$ in FIG. 2(a), n_{NP} increases with the pump rate and asymptotically reaches a maximum value of 6.22. FIG. 2(b) shows the spectral evolution of the nanoplasmons in color map as a function of the pump in logarithmic scale. The three panels from the bottom to the top show four distinct emission dynamics as the pump rate increases. (i) At very low pump in the lower panel, the emission from $|2\rangle \rightarrow |1\rangle$ exhibits

VRS feature as predicted by the Jaynes-Cummings model [44]. (ii) As the pump increases a bit, the Raman pump induced coherence $\hat{\sigma}_{12}$ emerges and then dominates over VRS, and emission spectra display features like a Mollow triplet [44]. The change is clearly seen around $\Omega = 0.1\kappa$. The appearance of the Mollow triplet can be explained through the dressed-state picture where the states $|1\rangle$ and $|2\rangle$ are dressed by the pumps Ω_{13} and Ω_{23} via the intermediate state $|3\rangle$. (iii) Displayed in the middle panel, the Mollow triplet feature gradually disappears as the pump increases, and a single peak at the center persists and broadens. The coherence built by the Raman pumps becomes weak as compared to the coherence due to the interaction with the nanoplasmions whose number increases with the pump. (iv) As nanoplasmions accumulate, stimulated emission dominates and a prominent line narrowing feature occurs. The asymptotic linewidth is about $\kappa/125$. FIG. 2(c) depicts the second-order intensity correlation function at zero delay $g^{(2)}(0)$. A clear plateau of $g^{(2)}(0) \sim 1.0$ shows up as Ω_{23} becomes large, indicating coherent nanoplasmion generation. In FIG. 2(d), we show the nanoplasmion occupation histogram for various Fock states at $\Omega = 100\kappa$. The distribution resembles a Poissonian distribution as denoted by the circles. This clearly shows that the output of our system has the same photon statistics as a conventional laser. For larger Ω , the photon statistics approaches to a perfect coherent state. We remark in passing that although $n_{NP} = 6.22$ at saturation might seem a moderate nanoplasmion number, our single-emitter nanoscopic light source delivers coherent photon streams at a remarkable rate of $n_{NP}\kappa\eta \sim 226$ THz to the far field, when taking into account $\eta = 60\%$ as the radiation efficiency of the antenna. Note that the emission rate of microlasers is typically in the order of Megahertz [35]. The pumping rates of $\Omega = 100\kappa$ correspond to light intensities about 500 GW/cm². For a diffraction limited light pulse with a 10 ps duration (long enough to reach the steady state for the system), the pumping rates translate into pulse energies of a few nJ, which is readily available with pulse lasers. The proposed device emits more than 2000 photons each excitation pulse and can dissipate possible heat between pulses. Thus the device should operate well in pulse mode with minimum heating problem.

Next we investigate in more detail the properties of the single-emitter nanoscopic light source and gain insight into the working principle. FIG. 3(a) and 3(b) respectively plot with color-coded traces n_{NP} and state $|2\rangle$ population $\langle\hat{\sigma}_{22}\rangle$ of the emitter for a series of coupling constants as a function of the pump rate. The populations of the atomic states are obtained from the diagonal elements of the reduced density matrix for the atomic part. For a fixed coupling constant, the trends of n_{NP} and $\langle\hat{\sigma}_{22}\rangle$ versus the pump are similar. In particular, for $g=100$ meV, the two green-dashed traces show a shoulder around $\Omega = 10\kappa$,

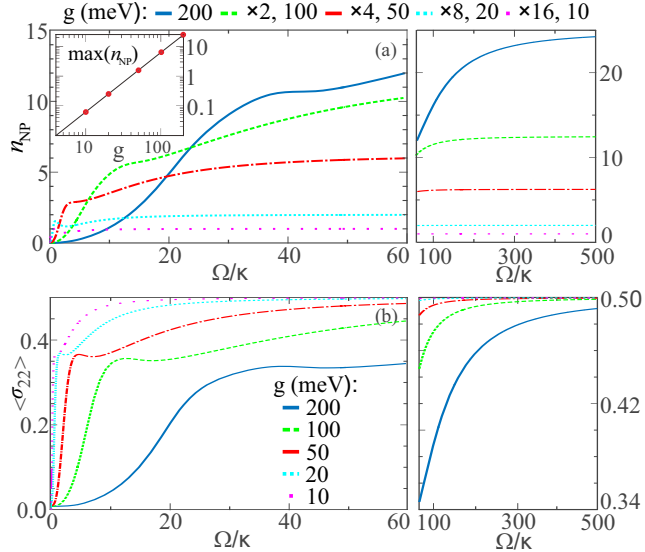


FIG. 3 (color online) Average nanoplasmon number (a) and population in state $|2\rangle$ (b) as functions of the pump rate Ω and coupling constant. The inset depicts the maximum nanoplasmon number v.s. coupling constant in double logarithmic scale.

which corresponds to a transition point in the spectrum evolution chart in the upper panel of FIG. 2(b). After the shoulder, the nanoplasmons enter a linear amplification regime where the stimulated emission plays a central role, accompanying line narrowing witnessed in FIG. 2(b). Before the shoulder, n_{NP} increases with the pump rate at a larger slope due to the fast increase of $\langle \hat{\sigma}_{22} \rangle$. In this regime, the populations of $|2\rangle$ and $|1\rangle$ are still not inverted (see appendix). We identify that n_{NP} is mostly related to $\langle \hat{\sigma}_{22} \rangle$, and population inversion is unnecessary for the accumulation of nanoplasmons. This is because when the inversion is negative the Raman pump scheme forms an efficient path ($|1\rangle \rightarrow |3\rangle \rightarrow |2\rangle$) to cycle the population from $|1\rangle$ to $|2\rangle$, and can be much faster than the direct simulated absorption ($|1\rangle \rightarrow |2\rangle$) by the nanoplasmons. The larger $\langle \hat{\sigma}_{22} \rangle$ is, the more the plasmons can accumulate. The above features are present for all coupling constants considered here. At very large pump, $\langle \hat{\sigma}_{22} \rangle$ saturates to 0.5 and the average nanoplasmon number asymptotically reaches the maximum value.

The saturation of the nanoplasmon number with the increase of the pump is a prominent difference from the self-quenching phenomena observed in microlasers [32], where the photon number in the cavity decreases at high pump rate due to the quenching of the coherence. The saturation behavior in our system can be understood from the perspective of power balance. The rate of power feeding the whole system is given by $W = -\frac{1}{2} \text{Re}\{i\omega_0 \langle \vec{p}^* \cdot \vec{E} \rangle\}$, where $\vec{p} = \vec{\mu} \hat{\sigma}_{12}$ is the induced dipole moment operator of the emitter and \vec{E} is the electric field operator at ω_0 at the emitter position near the antenna. It follows that

$\langle \vec{\mu} \cdot \vec{E} \rangle \propto \sqrt{n_{NP}} g$ and the power loss rate $\propto \hbar\omega_0 n_{NP} \kappa$. The feeding power and the loss should be balanced and consequently one obtains $n_{NP} \propto \left(\frac{g}{\kappa}\right)^2$. For a single emitter, the coherence $\langle \hat{\sigma}_{12} \rangle$ has a finite value and therefore there is an upper bound for the attainable plasmon number. In particular, for the three-level system with the Raman pumps, $\langle \hat{\sigma}_{12} \rangle$ asymptotically saturates to a value of -0.5 regardless of the coupling strength, and consequently the correlation of the coherence and field operators reaches a constant value. The inset of FIG.3(a) depicts the numerically calculated maximum n_{NP} as a function of coupling constant and the data can be well fitted by $n_{NP} = 0.97(g/\kappa)^2$. We obtain the photon emission rate $n_{NP}\kappa\eta$ of about 9 THz and 56 THz for coupling constants of 20 meV and 50 meV, respectively. In addition, the emissions remain coherent as indicated by the second-order intensity correlation functions (see appendix). The fact that for $g = 20$ meV the system delivers bright coherent photon streams shows that the single-emitter nanoscopic light source can operate at various levels of coupling, including the case where the system is not strongly coupled. With state-of-the-art nanofabrication and nanocontrol techniques [30,31], such systems should be realizable in the laboratory.

We have studied so far the nanoplasmon generation and radiation with a single emitter without additional dephasing channel other than spontaneous decay, which only holds for solid-state emitters at cryogenic temperatures. At higher temperatures, due to the system-environment interactions, solid-state emitters usually experience fast dephasing. For example, organic molecules at room temperatures may

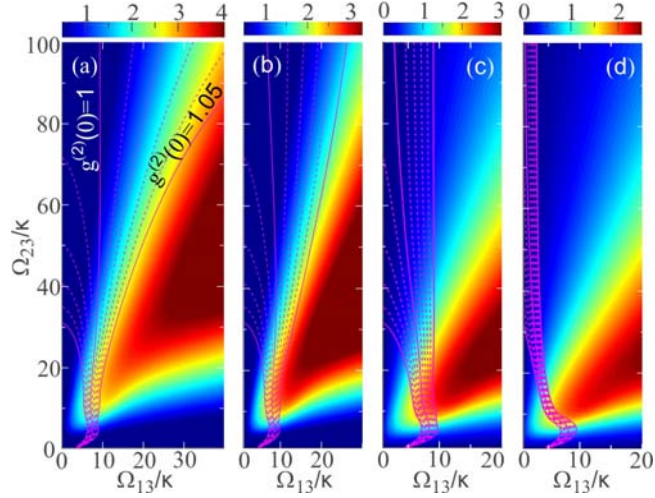


FIG. 4 (color online) Dephasing effect on average nanoplasmon number and second-order intensity correlation function at zero delay $g^{(2)}(0)$ for $g = 100$ meV. The dephasing rates are 10^{10} , 10^{11} , 10^{12} and 10^{13} s $^{-1}$ for (a), (b), (c) and (d), respectively. The contours of $g^{(2)}(0) = 0.95$ to 1.05 from left to right are overlaid on the graphs.

have coherence times of 100 fs. We now discuss the dephasing effect on the performance of the device. We introduce the dephasing γ_{de} to state $|2\rangle$ on top of spontaneous decay ($\gamma_e = 10^9 \text{ s}^{-1}$) and calculate the average nanoplasmon number and second-order intensity correlation function as functions of pump rates. Dephasing rates of 10^{10} s^{-1} , 10^{11} s^{-1} , 10^{12} s^{-1} and 10^{13} s^{-1} have been considered for $g = 100 \text{ meV}$ and the results are summarized in FIG. 4(a)–(d). The average nanoplasmon number is displayed in color maps as functions of pump rates, while the $g^{(2)}(0)$ contours with values from 0.95 to 1.05 are overlaid on the color maps. For the dephasing rate of 10^{10} s^{-1} illustrated in FIG. 4(a), the contours open up and the maximum plasmon number of $n_{NP} = 6.17$ is obtained with $g^{(2)}(0) \sim 1.0$. As dephasing rate becomes larger, the contour enclosed region shrinks and becomes a narrow band for the fastest dephasing. Within the banded region the maximum nanoplasmon number is obtained at some optimal pump rates. Working with the optimal pumps, the emission of the nanoscopic light source is nearly coherent and moderate average nanoplasmon numbers can still be secured, for example, $n_{NP} > 1.5$ for the fastest dephasing rate considered here ($\gamma_{de} = 10^{13} \text{ s}^{-1}$).

In this work we have proposed the generation and radiation of coherent nanoplasmons fueled by a single-emitter gain medium and investigated the emission properties of the device at various conditions. Under a Raman pump configuration, the pumps effectively expedite the process of populating the upper emitting level of the emitter in the presence of fast plasmon decay and increase the average number of nanoplasmons from otherwise far less than one to a macroscopic accumulation. We point out that the pumps do not need necessarily to be resonant with the emission levels [39] and the device should also work with incoherent pumps (see appendix). In the proposed system, the plasmonic nanoresonator provides deep-subwavelength field concentration in terms of nanoplasmons and at the same time efficiently funnels the energy of highly localized plasmons to far-field photons. With realistic parameters including the coupling constant, pumping rate and dephasing rate, our calculations show that the single-emitter nanoscopic source can deliver bright coherent photon streams with a rate of hundreds of Terahertz. The device should be realizable with solid-state emitters such as organic molecules in solids and quantum dots in pulsed mode with minimum heating problem at room temperature [3]. The proposed scheme bridges the size mismatch between optical active components and individual emitters, making it ideally suitable for integrated plasmonic circuitry [46]. The possibility of achieving nanoscale bright coherent emission with a single solid-state emitter has far-reaching implications for ultra-compact integration of

functional optoelectronic devices [4] and for the control of signals in quantum networks and metamaterials [47].

We acknowledge financial support from the National Natural Science Foundation of China (grant 11474114, 11604109), the Thousand-Young-Talent Program of China, Huazhong University of Science and Technology, and the Max Planck Society. X.-W. C acknowledges fruitful discussions with Z.-Y. Li, R.-M. Ma and M. Litinskaya. I. P. wishes to thank I.V. Smetanin and A. Uskov for discussions.

Appendix

In this appendix, we provide additional information for understanding the generation and radiation of coherent nanoplasmons powered by a single three-level quantum emitter on a plasmonic nanoresonator.

1. Evolution of the atomic population inversion with the pump

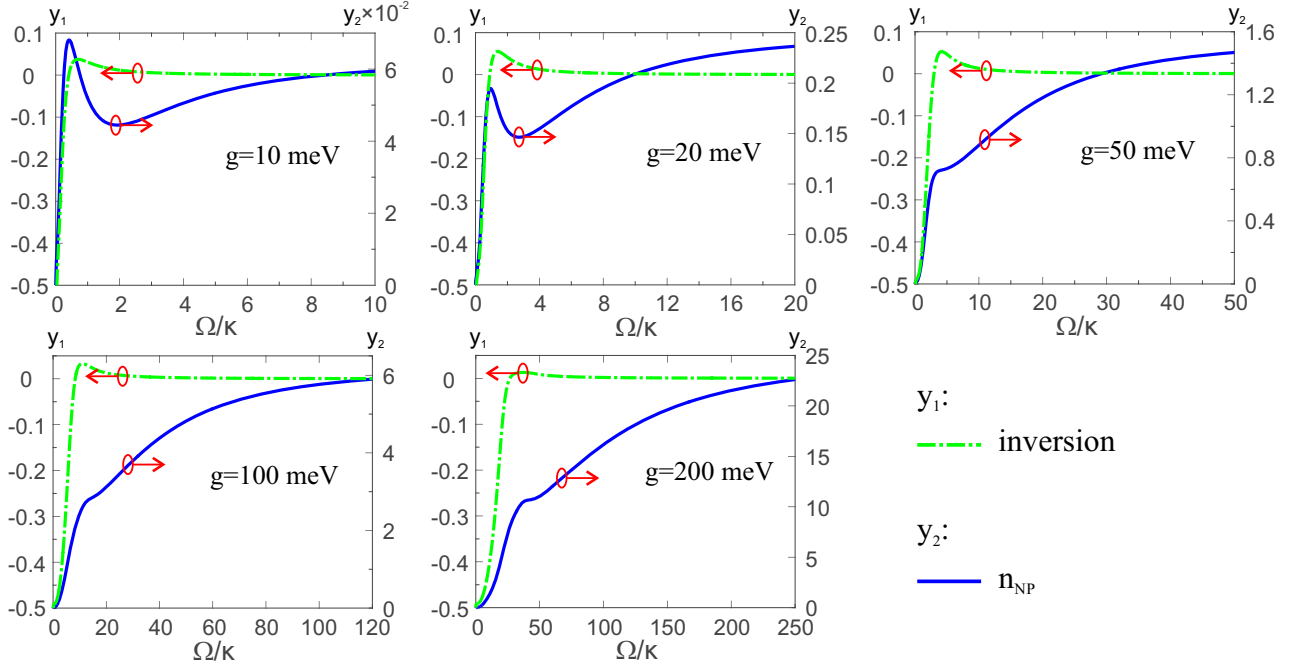


FIG. A1 (color online) The evolution of atomic population inversion and nanoplasmon number as functions of the pump rate Ω for various coupling constants.

The population difference (inversion) between $|2\rangle$ and $|1\rangle$ are plotted in FIG.A1 as functions of the pump rate $\Omega_{23} = \Omega_{13} = \Omega$ in the units of κ for a variety of emitter-plasmon coupling constants. The

average nanoplasmon numbers n_{NP} are also displayed as blue-solid lines in FIG.A1. Note that there are two vertical axes, i.e., the left one is for the atomic inversion and the right one is for n_{NP} . From these plots, one sees that for all the coupling constants n_{NP} increases from zero to a considerable value before the population inversion turns to be positive. After the population inversion becomes positive, there is further boost of the plasmon number as a result of more stimulated emission. We also observe local maxima in nanoplasmon number for $g = 10$ and 20 meV when the inversion crosses zero. Afterwards the inversion eventually approaches zero from above (keeping positive), while nanoplasmon number increases until saturation.

2. Second-order coherence property of plasmon emission for $g=10$ meV, 20 meV and 50 meV

Here we show that the emission has good coherence for small coupling strengths between the emitter and antenna as shown in FIG.1 of the main text. FIG.A2 plots in the color maps the second-order intensity correlation function at zero delay for $g = 10$ meV, 20 meV and 50 meV. One clearly observes that when the pump rate Ω_{23} is large enough the correlation function becomes essentially 1. As revealed by the contours, for stronger emitter-antenna coupling higher pump rates are required to guarantee good coherence.

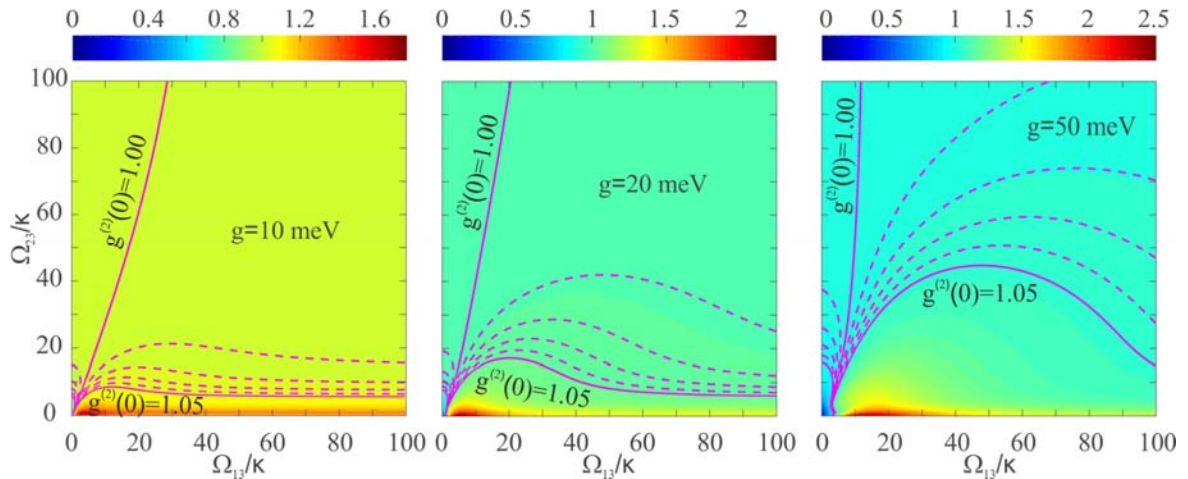


FIG. A2 (color online) Second-order correlation functions of the single-emitter nanoscopic coherent light source: the color maps of $g^{(2)}(0)$ for the coupling constants of 10 meV, 20 meV and 50 meV v.s. two pump rates are rendered. Contours of $g^{(2)}(0) = 0.95 \sim 1.05$ are overlaid on the color maps.

3. Generation and radiation of nanoplasmons with incoherent pump for the $|3\rangle \rightarrow |2\rangle$ transition

We show that the generation and radiation of coherent nanoplasmons with a single emitter still work when the coherent pump Ω_{23} is replaced by an incoherent pump with rate Γ for $|3\rangle \rightarrow |2\rangle$ transition.

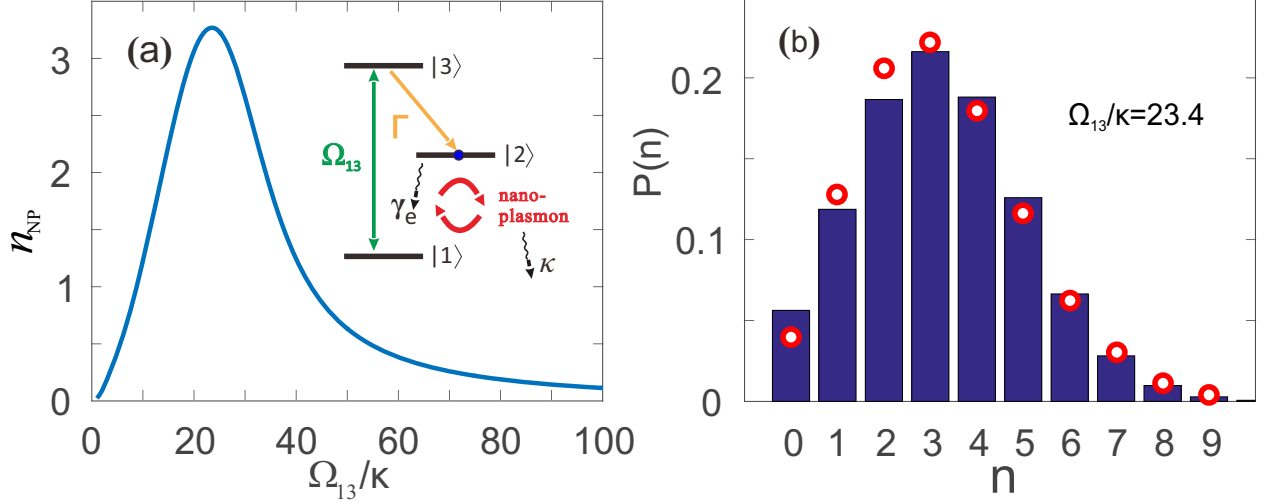


FIG. A3 (color online) Nanoplasmon generation and radiation with an incoherent pump of the $|3\rangle \rightarrow |2\rangle$ transition rate $\Gamma = 40\kappa$ and coupling constant $g = 100$ meV: (a) average plasmon number as a function of pump rate Ω_{13} . (b) Fock state occupation of the nanoplasmons ($\Omega_{13} = 23.4\kappa$) compared with Poissonian distribution (circles).

The schematic diagram is shown as inset in FIG.A3(a) and the dynamics of the system is governed by the master equation in Lindblad form[32,44]

$$\dot{\hat{\rho}} = \frac{i}{\hbar} [\hat{\rho}, \mathcal{H}_I] + \mathcal{L}\{\sqrt{\gamma_e} \hat{\sigma}_{12}\} + \mathcal{L}\{\sqrt{\gamma_{de}} \hat{\sigma}_{22}\} + \mathcal{L}\{\sqrt{\kappa} \hat{a}\} + \mathcal{L}\{\sqrt{\Gamma} \hat{\sigma}_{23}\}, \quad (\text{A.1})$$

with the Hamiltonian

$$\mathcal{H}_I = \hbar g(\hat{a}^\dagger \hat{\sigma}_{12} + \hat{\sigma}_{21} \hat{a}) + \frac{1}{2} \hbar \Omega_{13}(\hat{\sigma}_{13} + \hat{\sigma}_{31}). \quad (\text{A.2})$$

We assume there is fast incoherent pump $\Gamma = 40\kappa$ from $|3\rangle \rightarrow |2\rangle$. The performance is demonstrated in FIG.A3 for the nanoscopic coherent light source with the coupling constant $g = 100$ meV. With this incoherent pump rate, the trace in FIG.A3(a) shows the average nanoplasmon number as a function of the coherent pump Ω_{13} in the units of κ . In this case, one observes a maximum number for $n_{NP} = 3.23$ as the pumping rate increases to 23.4κ and then n_{NP} decreases eventually to zero as the pump rate becomes even larger, which is due to the pumping self-quenching effect as observed in microlasers [32]. FIG.A3(b) displays the nanoplasmon number occupation distribution in the Fock state space for $\Omega_{13} =$

23.4κ. The circles indicate the Poissonian distribution and one clearly observes a good agreement between the two, which confirms that the emission is coherent, like a laser. The rate of the incoherent pump should be fast enough to guarantee the occupation of state $|2\rangle$ in case of strong coupling and fast decay of the nanoplasmons.

References

1. A.E. Siegman, Lasers, University Science Books, Sausalito, CA (USA) (1986).
2. P. Berini, I. De Leon, Surface plasmon-polariton amplifiers and lasers, *Nat. Photonics* **6**, 16 (2012).
3. O. Hess, J.B. Pendry, S.A. Maier, R.F. Oulton, J.M. Hamm and K.L. Tsakmakidis, Active nanoplasmonic metamaterials, *Nat. Mater.* **11**, 573 (2012).
4. M.T. Hill, M.C. Gather, Advances in small lasers, *Nat. Photonics* **8**, 908 (2014).
5. D.J. Bergman and M.I. Stockman, Surface plasmon amplification by stimulated emission of radiation: Quantum generation of coherent surface plasmons in nanosystems, *Phys. Rev. Lett.* **90**, 027402 (2003).
6. I.E. Protsenko, A.V. Uskov, O.A. Zaimidoroga, V.N. Samoilov and E.P. O'Reilly, Dipole nanolaser, *Phys. Rev. A* **71**, 063812 (2005).
7. N.I. Zheludev, S.L. Prosvirnin, N. Papasimakis, V.A. Fedotov, Lasing spaser, *Nat. Photonics* **2**, 351 (2008).
8. M. Stockman, Spaser explained, *Nat. Photonics* **2**, 327 (2008).
9. S.-W. Chang, C.-Y.A. Ni, S.L. Chuang, Theory for bowtie plasmonic nanolasers, *Opt. Express* **16**, 10580 (2008).
10. M.A. Noginov, G. Zhu, A.M. Belgrave, R. Bakker, V.M. Shalaev, E. Narimanov, S. Stout, E. Herz, T. Suteewong and U. Wiesner, Demonstration of a spaser-based nanolaser, *Nature* **460**, 1110 (2009).
11. R.F. Oulton, V.J. Sorger, T. Zentgraf, R.-M. Ma, C. Gladden, L. Dai, G. Bartal and X. Zhang, Plasmon lasers at deep subwavelength scale, *Nature* **461**, 629 (2009).
12. R.-M. Ma, R.F. Oulton, V.J. Sorger, G. Bartal and X. Zhang, Room-temperature sub-diffraction-limited plasmon laser by total internal reflection, *Nat. Materials* **10**, 110 (2011).
13. Y.-J. Lu, J. Kim, H.-Y. Chen, C.H. Wu, N. Dabidian, C.E. Sanders, C.-Y. Wang, M.-Y. Lu, B.-H. Li, X. Qiu, W.-H. Chang, L.-J. Chen, G. Shvets, C.-K. Shih and S. Gwo, Plasmonic nanolaser using epitaxially grown silver film, *Science* **337**, 450 (2012).
14. K. Ding, Z.-C. Liu, L.-J. Yin, M.T. Hill, M.J.H. Marell, P.J. van Veldhoven, R. Noetzel and C.-Z. Ning, Room-temperature continuous wave lasing in deep-subwavelength metallic cavities under electrical injection, *Phys. Rev. B* **85**, 041301 (R) (2012).
15. W. Zhou, M. Dridi, J.-Y Suh, C.-H Kim, D.T. Co, M.R. Wasielewski, G.C. Schatz and T.W. Odom, Lasing action in strongly coupled plasmonic nanocavity arrays, *Nat. Nanotech.* **8**, 506 (2013).
16. X. Meng, J.-J. Liu, A.V. Kildishev and V.M. Shalaev, Highly directional spaser array for the red wavelength region, *Laser Photonics Rev.* **8**, 896 (2014).
17. M. Agio and A. Alu, Editors, Optical Antennas, Cambridge University Press, New York (2013).
18. J.J. Greffet, Nanoantennas for light emission, *Science* **308**, 1561 (2005).
19. L. Rogobete, F. Kaminski, M. Agio, V. Sandoghdar, Design of plasmonic nanoantennae for enhancing spontaneous emission, *Opt. Lett.* **32**, 1623 (2007).

20. A.G. Curto, G. Voipe, T.H. Taminiau, M.P. Kreuzer, R. Quidant and N.F. Hulst, Unidirectional emission of a quantum dot coupled to a nanoantenna, *Science* **329**, 930 (2010).
21. Y. Gu, L.-J. Wang, P. Ren, J.-X. Zhang, T.-C. Zhang, O.J.F. Martin and Q.-H. Gong, Surface-plasmon-induced modification on the spontaneous emission spectrum via subwavelength-confined anisotropic Purcell factor, *Nano Lett.* **12**, 2488 (2012).
22. X.-W. Chen, M. Agio and V. Sandoghdar, Metallodielectric hybrid antennas for ultrastrong enhancement of spontaneous emission, *Phys. Rev. Lett.* **108**, 233001 (2012).
23. M. Agio, Optical antennas as nanoscale resonators, *Nanoscale* **4**, 692 (2012).
24. C. Sauvan, J.P. Hugonin, I.S. Maksymov and P. Lalanne, Theory of the spontaneous optical emission of nanosize photonic and plasmon resonators, *Phys. Rev. Lett.* **110**, 237401 (2013).
25. A. Trügler and U. Hohenester, Strong coupling between a metallic nanoparticle and a single molecule, *Phys. Rev. B* **77**, 115403 (2008).
26. S. Savasta, R. Saija, A. Ridolfo, O.D. Stefano, P. Denti and F. Borghese, Nanopolaritons: Vacuum Rabi splitting with a single quantum dot in the center of a dimer nanoantenna, *ACS Nano* **4**, 6369 (2010).
27. A. Ridolfo, O. Di Stefano, N. Fina, R. Saija and S. Savasta, Quantum plasmonics with quantum dot-metal nanoparticle molecules: Influence of the Fano effect on photon statistics, *Phys. Rev. Lett.* **105**, 263601 (2010).
28. A. Manjavacas, F.J. García de Abajo and P. Nordlander, Quantum plexcitonics: Strongly interacting plasmons and excitons, *Nano Lett.* **11**, 2318 (2011).
29. R.-Q. Li, D. Hernández-Pérez, F. J. García-Vidal and A. I. Fernández-Domínguez, Transformation optics approach to plasmon-exciton strong coupling in nanocavities, *Phys. Rev. Lett.* **117**, 107401 (2016).
30. R. Chikkaraddy, B. de Nijs, F. Benz, S.J. Barrow, O.A. Scherman, E. Rosta, A. Demetriadou, P. Fox, O. Hess and J.J. Baumberg, Single-molecule strong coupling at room temperature in plasmonic nanocavities, *Nature* **535**, 127 (2016).
31. K. Santhosh, O. Bitton, L. Chuntonov and G. Haran, Vacuum Rabi splitting in a plasmonic cavity at the single quantum emitter limit, *Nat. Comm.* **7**, 11823 (2016).
32. Y. Mu and C. M. Savage, One-atom lasers, *Phys. Rev. A* **46**, 5944 (1992).
33. P.R. Rice and H.J. Carmichael, Photon statistics of a cavity-QED laser: A comment on the laser-phase-transition analogy, *Phys. Rev. A* **50**, 4318 (1994);
34. M. Löffler, G.M. Meyer and H. Walther, Spectral properties of the one-atom laser, *Phys. Rev. A* **55**, 3923 (1997).
35. J. McKeever, A. Boca, A.D. Boozer, J.R. Buck and H.J. Kimble, Experimental realization of a one-atom laser in the regime of strong coupling, *Nature* **425**, 268 (2003).
36. O. Astafiev, K. Inomata, A.O. Niskanen, T. Yamamoto, Y.A. Pashkin, Y. Nakamura and J.-S. Tsai, Single artificial-atom lasing, *Nature* **449**, 588 (2007).
37. M. Nomura, N. Kumagai, S. Iwamoto, Y. Ota and Y. Arakawa, Laser oscillation in single-quantum-dot-nanocavity system, *Nat. Phys.* **6**, 279 (2010).
38. A. Moelbjerg, P. Kaer, M. Lorke, B. Tromborg and J. Mørk, Dynamical properties of nanolasers based on few discrete emitters, *IEEE J. Sel. Top. Quantum Electron.* **49**, 945 (2013).
39. Y. Wu, Effective Raman theory for a three-level atom in the Λ configuration, *Phys. Rev. A* **54**, 1586 (1996).
40. T. Savels, A.P. Mosk and Ad Lagendijk, Gain narrowing in few-atom systems, *Phys. Rev. Lett.* **98**, 103601 (2007).

41. P. Atkins, J. de Paula, *Physical Chemistry*, 10th Edition, Oxford University Press, Oxford, United Kingdom (2014).
42. S.W. Hell and J. Wichmann, Breaking the diffraction resolution limit by stimulated emission: Stimulated-emission-depletion fluorescence microscopy, *Opt. Lett.* **19**, 780 (1994).
43. A. Mohammadi, F. Kaminski, V. Sandoghdar and M. Agio, Fluorescence enhancement with the optical (bi-) conical antenna, *J. Phys. Chem. C* **114**, 7372 (2010).
44. J.C. Garrison and R.Y. Chiao, *Quantum Optics*, Oxford University Press, Oxford (2008).
45. C.W. Gardiner, *Quantum Noise*, Springer-Verlag, Berlin (1991).
46. Y. Fang and M. Sun, Nanoplasmonic waveguides: Towards applications in integrated nanophotonic circuits, *Light: Sci. Appl.* **4**, 294 (2015).
47. M.S. Tame, K.R. McEnergy, S.K. Özdemir, J. Lee, S.A. Maier and M.S. Kim, Quantum plasmonics, *Nat. Phys.* **9**, 329 (2013).